Modeling and Optimization of High Temperature Proton Exchange Membrane Electrolyzer Cells

Dongqi Zhao [a], Qijiao He [b], Xiaolong Wu [a], Yuanwu Xu [a], Jianhua Jiang [a], Xi Li [a]*,

Meng Ni [b]*

Highlights:

- The effect of voltage, anode gas composition, anode gas velocity, and cathode gas velocity on the multiphysics field are studied.
- The efficiency and conversion rate are predicted under different operating conditions.
- The optimal operating point is found to achieve maximum energy efficiency.

Modeling and Optimization of High Temperature Proton Exchange Membrane Electrolyzer Cells

Dongqi Zhao [a], Qijiao He [b], Xiaolong Wu [a], Yuanwu Xu [a], Jianhua Jiang [a], Xi Li [a]*, Meng Ni [b]*

a. School of Artificial Intelligence and Automation, Key Laboratory of Image Processing and Intelligent Control of Education Ministry, Huazhong University of Science and Technology, Wuhan, Hubei, China.

b. Building Energy Research Group, Department of Building and Real Estate, The Hong Kong Polytechnic University, Hung Hom, Kowloon, Hong Kong.

*Corresponding author: Xi Li and Meng Ni.

E-mail address: lixi_wh@126.com (Xi Li), meng.ni@polyu.edu.hk (Meng Ni)

Abstract

Although high temperature proton exchange membrane electrolyzer cells (HT-PEMECs) are promising devices to store energy in recent years, the effect of certain parameters on the performance is still unclear. Therefore, a 2D multiphysics model is adopted to study the related processes of the electrochemical reaction in an HT-PEMEC. The model is validated by comparison with electrochemical experimental data. Subsequently, the effects of applied voltage, anode water mass fraction, anode gas velocity, and cathode gas velocity on the multiphysics are studied, and the trends of efficiency and conversion rate are analyzed. Thermoneutral voltage is observed through a parametric study. Moreover, maximum energy efficiency (54.5%) is obtained by optimizing operating conditions. This study can be regarded as a foundation for the subsequent control and multi-objective optimization research.

Keywords: Multiphysics model; Proton exchange membrane electrolyzer cell; High temperature electrolysis; Optimal operating conditions; Energy efficiency.

1. Introduction

Sustainable and clean energy technologies are eagerly needed to solve serious environmental problems and to meet human demands [1-2]. Although the utilization of renewable energy can alleviate energy demand, they are site-specific, intermittent, and are thus not reliable. To wider and more reliable applications of renewable energy technologies, effective energy storage is critical. Hydrogen is a hopeful energy carrier for renewable power storage. Excess renewable power can be used to drive an electrolyzer for generating hydrogen, which not only can be used in the chemical industry but also be transformed into electricity by a fuel cell when renewable power cannot meet demand [3-9]. In addition, hydrogen is an ideal fuel for fuel cells to achieve low-emission and smart transport, and related fields have been extensively researched.

Proton exchange membrane electrolyzer cell (PEMEC) that works at low temperature is a promising electrochemical cell for hydrogen production from water [10-12]. The high proton conductivity of membrane requires a high water content, the operation temperature is usually below 100℃ unless the system is pressurized to maintain sufficient hydration of the membrane [13-14]. However, at a temperature of below 100℃, the energy input to a PEMEC is electricity and the contribution by thermal energy is very low. More importantly, the sluggish reaction kinetics at the electrodes require the use of expensive catalysts such as Pt, making the PEMEC very expensive. With the development of alternative electrolyte membranes, it is possible to operate a PEMEC at a temperature of above 100℃, which is desirable for hydrogen production due to multiple reasons [15-16]. First, the electrode kinetics increases when the operating temperature is increasing, reducing the activation overpotentials of the electrode and enabling the use of lower-cost catalysts. Secondly, for steam electrolysis at 130℃, the total energy

requirement for the electrochemical reaction (△H) is 243 kJ mol^{-1}, lower than that for electrolytic reaction at 80°C (284 kJ mol^{-1}). Third, the reversible electric potential calculated through the Gibbs free energy change (△G), can be slightly decreased by raising the operating temperature of the electrolyzer from 80℃ (1.18 V) to 130℃ (1.16 V). Accordingly, HT-PEMEC requires more thermal energy input, indicating that more waste heat can be used for hydrogen production by an HT-PEMEC.

Compared with high temperature solid oxide electrolyzer cells (SOECs) working at a temperature range of 600-800°C, HT-PEMEC is also advantageous as a wider range of waste heat can be used in HT-PEMEC. Moreover, high temperature SOECs suffer from relatively poor durability due to the high temperature sintering of the porous electrodes. The startup and shutdown of SOECs are time-consuming and the operation of SOEC is less flexible. Therefore, HT-PEMECs are very promising for hydrogen production and have received increasing attention in recent years.

Although a few experimental studies on hydrogen production by HT-PEMECs have been reported, very few papers on the mathematical modelling of HT-PEMEC can be referenced. Diego et al. [17] adopted a model for HT-PEMEC to explore the effect of flow channel configurations on overall performance. They compared three different flow channel configurations in terms of hydrogen mole fraction, polarization curve, system average temperature and pressure drop. It is found that the multiple-serpentine channel is an optimal flow channel configuration. Li et al. [35] studied three different modes of flow fields (serpentine, parallel, and cascade), and analyzed their current-voltage characteristics and impedance. The experimental results show that the anodic flow channel mode mainly impacts the polarization loss related to the shortage of water in the catalyst layer, while the cathodic flow channel pattern only affects the ohmic loss. Li et al. [36] conducted experiments to explore the effect of temperature and pressure on HT-PEMEC. It is observed that an increase in

temperature does not increase the ohmic overpotential, but increases the concentration overpotential. It was also found that the overpotential caused by the temperature increase can be suppressed by increasing the operating pressure. Toghyani et al. [37] established a numerical model to study the effects of operating temperature, pressure, GDL thickness, and membrane thickness on exergy efficiency and cost. Xu et al. [38] tested the performance of HT-PEMEC and the experimental temperature is between 80 ℃ and 130 ℃ and the pressure is between 0.4 bar and 5 bar. S.Toghyani et al. [18] explored the effect of pressure, operating temperature and structural parameters such as membrane thickness, gas diffusion layer thickness and gas diffusion layer porosity, on the performance of the electrolyzer. In another study, Santarelli et al. [19] studied the effects of operating pressure and temperature on a high pressure PEMEC under different operating conditions using a non-isothermal model. It is found that pressure and temperature are crucial parameters for the overall performance of the high-pressure electrolyzer. Nafchi F M et al. [20] adopted an HT-PEMEC model coupled with thermal energy storage and concentrating solar power to investigate the system performance. They investigated the impact of the structural parameters of electrolyzer on the electrical efficiency and exergy of the system, and believed that system integration is an effective way to improve efficiency. Tijani AS et al. [21] establish the CFD model of the PEM electrolyzer, and the performance of the electrolyzer was improved by optimizing the structure of the bipolar plate.

The pioneering studies on the modelling of HT-PEMEC mentioned above focus on the flow channel design, cell structural parameters optimization and the high-pressure operation of HT-PEMEC. However, the effects of the operating parameters on the electrolyzer performance are still unknown, such as the operating voltage, inlet gas flow rate and inlet gas composition etc. It should be noted that the energy efficiency of HT-PEMEC has not been discussed in the previous modelling studies, which is critical for the identification of the optimal HT-PEMEC operation conditions. To fill the research gap, this paper aims to gain a fundamental

understanding of the coupled electrochemical reaction and transport processes in an HT-PEMEC with a focus on the operating parameter effects on HT-PEMEC efficiency. Moreover, the temperature distribution and reactant gas concentration distribution are analyzed to explore thermal safety and reactant starvation issues. The results of this study supplement the existing literature on HT-PEMEC and can be regarded as a fundamental understanding of the subsequent optimization and application research.

2. Model description

This numerical model developed is extended from our previous work for the transient process of HT-PEMEC and had been well-validated using experimental data [33] and reported in our previous work [34]. Therefore, this section introduces the model in brief.

The numerical steady-state model is applied to study the electrolysis reaction, electron and proton transport process, heat transport process, mass transport process, and momentum transport process in an HT-PEMEC. The schematic representation of the HT-PEMEC is shown in Fig.1, which includes the positive electrode-electrolyte-negative electrode assembly (PEN) and channels. The stream of the cathode and anode is set to steam, but in section 3.3 the anode stream is a mixture of steam and nitrogen to explore the effect of reactant concentration on efficiency. Furthermore, the model formulated in this study simulates the electrochemical reaction of electrolysis water to generate H_2 and O_2 under different operating conditions. The H_2O molecules undergo endothermic electrochemical reduction to form H_2 in the cathode and O_2 in the anode. In the literature on HT-PEMEC simulation [14], usually air is used as a carrier gas in the cathode, which is not practical as subsequent gas separation of H_2 from the air/H_2 mixture is needed. Therefore, in this study, steam is utilized as a carrier gas in the cathode as steam can be easily removed by condensation. Of course, the condensation heat must be well

utilized to avoid significant energy loss in practical operation.

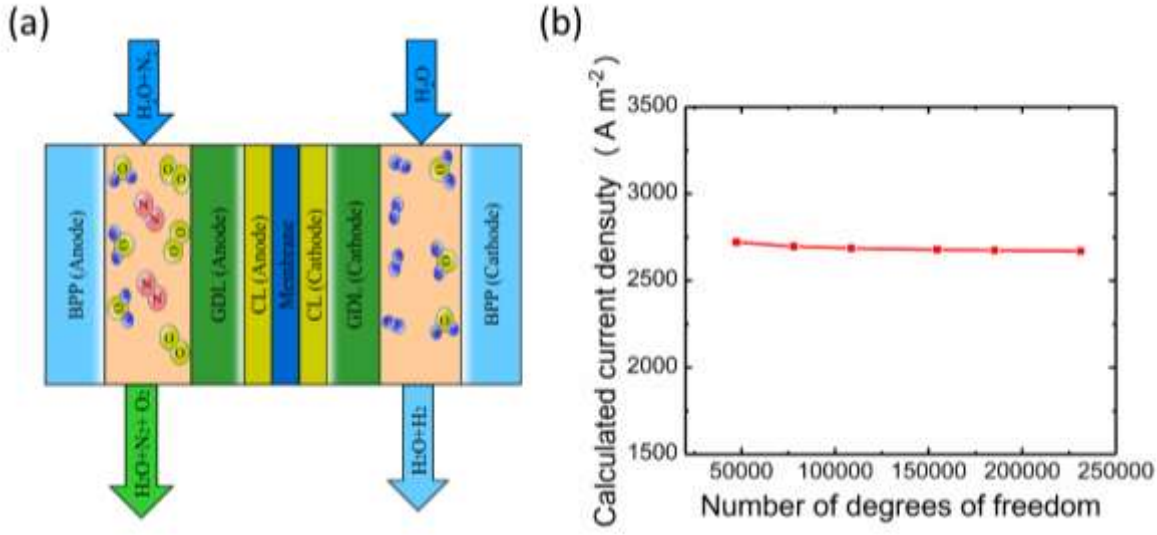

Fig.1 (a) Schematic of the HT-PEMEC; (b) Mesh independence validation.

2.1 Model assumption

The main model assumptions of HT- PEMEC are shown below.

(1) The reaction sites are evenly distributed at the catalyst layer, nonetheless, the electrochemical reaction rate is obviously different. The electrode-electrolyte interface possesses the highest reaction rate while that drops significantly away from the interface.

(2) The protonic and electronic charge transports of HT-PEMEC occur in PEN.

(3) All gas species are considered as ideal gases in this model, and the flow is considered incompressible.

2.2 Electrochemical reaction model

As presented in Fig.1, the electrolysis reaction can be regarded as two half-reactions at the anode and cathode which are described as Eqs. (1) and (2).

$$\text{Anode reaction:} \quad 2H_2O \rightarrow O_2 + 4H^+ + 4e^- \tag{1}$$

$$\text{Cathode reaction:} \quad 2H^+ + 2e^- \rightarrow H_2 \tag{2}$$

In electrolysis reaction, the operating potential (V) of HT-PEMEC can be written as [17]:

$$\mathrm{V} = \mathrm{E} + \eta_{act,an} + \eta_{act,ca} + \eta_{ohmic} \tag{3}$$

Here E represents the Nernst potential under the operating conditions; η_{act} is defined as the activation overpotentials (also called activation polarization) related to the electrolytic activity of the electrodes; η_{ohmic} is the ohmic polarization due to electronic and protonic conduction.

In an HT-PEMEC, the equilibrium potential of the electrochemical reaction can be expressed by Eq.(4), which includes the concentration overpotentials due to gas transport. Because gas partial pressure at TPB instead of the electrode surface is utilized, concentration loss is included in the equilibrium potential.

$$\mathrm{E} = E^0_{H_2} + \frac{RT}{2F} ln \left[\frac{P^L_{H_2} \left(P^L_{O_2}\right)^{1/2}}{P^L_{H_2O}} \right] \tag{4}$$

Here $E^0_{H_2}$ is defined as the equilibrium potential under standard conditions. R and T represent the universal gas constant and operating temperature. $P^L_{H_2}$, $P^L_{H_2O}$, and $P^L_{O_2}$ denote the partial pressures of component gas at TPB, respectively. F denotes the Faraday constant. Further, the value of E^0 for H_2 can be expressed by Eq. (5) as:

$$E^0_{H_2} = 1.253 - 0.00024516T\ (V) \tag{5}$$

Therefore, the Nernst potentials of HT-FEMEC can be written by combining Eqs. (4) and (5) as:

$$\mathrm{E} = 1.253 - 0.00024516\mathrm{T} + \frac{RT}{2F} ln \left[\frac{P^L_{H_2} \left(P^L_{O_2}\right)^{1/2}}{P^L_{H_2O}} \right] (V) \tag{6}$$

The activation overpotentials are the potential loss reflecting the activation energy barrier for the electrolysis reaction. The relationship between the current density and the activation overpotentials can be described by the Butler-Volmer equation [22-24].

$$\mathrm{i} = i_0 \left\{ exp\left(\frac{\alpha n F \eta_{act}}{RT}\right) - exp\left(\frac{(1-\alpha) n F \eta_{act}}{RT}\right) \right\} \tag{7}$$

Here i and i_0 represent the operating current density (A cm^{-2}) and the exchange current density (A cm^{-2}), respectively. α denotes the electronic transfer coefficient. n represents the number of electrons transferred. Moreover, the exchange current density i_0 of the electrolytic reaction can be further described as:

$$i_0 = \gamma exp\left(-\frac{E_{act}}{RT}\right) \tag{8}$$

Here γ (A m^{-2}) is defined as the pre-exponential factor and E_{act} represent the activation energy.

The ohmic overpotentials (η_{ohmic}) is described using Ohm's law, and the detailed calculation procedures can refer to Ref. [25].

2.3 Flow field and mass transport model

The process of gas mass transport in the porous media and channels can be described by Fick's model as presented in Eq. (9) [26].

$$N_i = -\frac{1}{RT}\left(\frac{B_o y_i P}{\mu}\nabla P - D_i^{eff}\nabla(y_i P)\right)(\text{i=1,…..,n}) \tag{9}$$

Here B_0 and μ represent the permeability of the porous media and gas viscosity, respectively. y_i is the molar fraction of gas component i. D_i^{eff} is defined as the overall effective transfer coefficient of component i. Moreover, D_i^{eff} can be expressed by Eq. (11) for gaseous species transport in the porous materials [27]:

$$D_i^{eff} = \frac{\varepsilon}{\tau}\left(\frac{1}{D_{im}^{eff}} + \frac{1}{D_{ik}^{eff}}\right) \tag{10}$$

Where ε and τ represent the porosity and tortuosity factor. More detailed description about D_{im}^{eff} and D_{ik}^{eff} can refer to Ref. [28]. Furthermore, the mass conservation law of HT-PEMFC can be expressed by Eq. (11) as:

$$\nabla\left(-D_i^{eff}\nabla c_i\right) = R_i \tag{11}$$

Here c_i denotes the molar concentration of gas component i. R_i is defined as the mass sources of different gas.

The classic Navier-Stokes equation with Darcy's term can be utilized to describe the gaseous species momentum in channels and porous materials as presented in Eq. (12) [29]:

$$\rho\frac{\partial \mathrm{u}}{\partial \mathrm{t}} + \rho \mathrm{u}\nabla \mathrm{u} = -\nabla \mathrm{p} + \nabla\left[\mu(\nabla \mathrm{u} + (\nabla \mathrm{u})^T) - \frac{2}{3}\mu\nabla \mathrm{u}\right] - \frac{\varepsilon\mu \mathrm{u}}{B_0} \quad (12)$$

2.4 Heat transfer model

In an HT-PEMEC, the electrolysis reaction at the reaction sites (TPB) consume heat while irreversible losses generate heat, and the temperature gradient along the gas flow direction is affected by heat changes [30]. Therefore, the classical heat balance equation can be used to describe the heat transfer process in an HT-PEMEC as:

$$\rho C_p u \bullet \nabla T + \nabla\left(-\lambda_{eff}\nabla T\right) = Q \quad (13)$$

Here C_p and u are defined as the heat capacity of the fluid and fluid velocity, respectively. λ_{eff} denotes the effective thermal conductivity. Q is the thermal source term, which represents the heat consumption and generation due to the electrolysis reaction and polarization losses. Furthermore, λ_{eff} can be expressed by Eq.(15) at the porous structure of electrodes [31]:

$$\lambda_{eff} = (1-\varepsilon)\lambda_s + \varepsilon\lambda_l \quad (14)$$

Here λ_s and λ_l represent the thermal conductivity of the solid and liquid phases. Furthermore, the detailed model parameters are shown in Table 1.

Table 1. Multiphysics model parameters.

Parameter	Value	Unit
Channel height	1	mm
Channel length	20	mm
Channel width	1	mm
Catalyst layer thickness	0.05	mm

Gas diffusion layer thickness	0.38	mm
Membrane thickness	0.1	mm
Gas diffusion layer length	20	mm
Catalyst layer length	20	mm
Membrane length	20	mm
Catalyst layer porosity	0.3	
GDL porosity	0.4	
Operating temperature	403.15	K
Operating pressure	1	bar
Electrode permeability	2.36×10^{-12}	m^2
GDL permeability	1.18×10^{-11}	m^2
Proton conductivity of electrolyte	20	$S\ m^{-1}$
Anode exchange current density	10^{-4}	$A\ cm^{-2}$
Cathode exchange current density	0.1	$A\ cm^{-2}$
Anode transfer coefficient	0.2	
Cathode transfer coefficient	0.5	
Viscosity of hydrogen	$(27.758+2.12E\text{-}1*T\text{-}3.28E\text{-}5*T^2)*1E\text{-}7$	Pa s
Thermal conductivities of hydrogen	$0.03591+4.5918E\text{-}4*T\text{-}6.4933E\text{-}8*T^2$	$W\ m^{-1}\ K$
Viscosity of oxygen	$(44.224+5.62E\text{-}1*T\text{-}1.13E\text{-}5*T^2)\ *1E\text{-}7$	Pa s
Thermal conductivities of oxygen	$0.00121+8.6157E\text{-}4*T\text{-}1.3346E\text{-}8*T^2$	$W\ m^{-1}\ K$
Viscosity of steam	$(-36.826+4.29E\text{-}1*T\text{-}1.62\ E\text{-}5*T^2)*\ 1E\text{-}7$	Pa s
Thermal conductivities of steam	$0.00053+4.7093E\text{-}4*T+4.9551E\text{-}8*T^2$	$W\ m^{-1}\ K$

2.5 Boundary conditions and model solution

For the electrolysis reaction, the potentials of electrodes are specified at outer boundaries. The potential at the boundary of the anode is applied voltage and that of the cathode is zero potential. Furthermore, insulation condition is considered at the top and bottom of HT-PEMFC. The mass fractions of gas species are specified at both inlets of the anode channel and cathode

channel. In addition, the electrode-electrolyte interface and the ends of the electrodes are set as zero flux. The gas flow rates are specified at both inlets of the cathode channel and anode channel. However, pressure conditions are specified at the outlet of the cathode channel and anode channel. The electrode-electrolyte interface and the ends of electrodes are the no-slip conditions. The detailed boundary values are listed in Table 2.

Table 2. Boundary value.

Boundary surface	Conditions
Gas inlet	$Y_{ca.H20} = 1$; $Y_{an.H20} = 1$; $Y_{an.N2} = 0$; $T_0 = 403.15$ K ; $u_{ca} = 0.4$ m s^{-1}; $u_{an} = 0.1$ m s^{-1};
Gas outlet	$P_0 = 1\ atm$
Anode outer surface	$\emptyset_{an} = V_{cell}$
Cathode outer surface	$\emptyset_{ca} = 0$
Remaining outer boundary	Adiabatic

In the subsequent parametric study, the corresponding parameter is adjusted to explore its impact on the multiphysics, while other operating parameters remained constant. The 2D numerical model is solved at different operating conditions by MUMPS solver, and the commercial software COMSOL MULTIPHYSICS® is used to calculate the multiphysics model.

2.6 Performance metrics

Suitable parameters need to be defined to characterize the performance of HT-PEMFC. The overall efficiency η and net syngas yield γ_{syn} are employed in this study for evaluating the electrolyzer performance. The overall efficiency of HT-PEMFC is defined as the ratio of the output energy to the input energy. The output energy is the total heat of the hydrogen

generation, while the input energy includes two source terms. One of them comes from the electrical power supplied, and the other is used to heat gas species from the ambient temperature to the specified inlet temperature.

$$\eta = \frac{(\dot{m}_{o,H_2} - \dot{m}_{i,H_2}) LHV_{H_2}}{V \int_0^{L_{RU}} i dz + \dot{m}_{i,ca} \int_{T_0}^{T_{i,ca}} C_{p,g,ca} dT + \dot{m}_{i,an} \int_{T_0}^{T_{i,an}} C_{p,g,an} dT} \quad (15)$$

Here the hydrogen mass flow rates at the outlet and inlet are expressed as $\dot{m}_{o,H_2}$ and $\dot{m}_{i,H_2}$ L_{RU} is the channel width. The mass flow rates of the component gas at the cathode and anode inlet are $\dot{m}_{i,ca}$ and $\dot{m}_{i,an}$. $C_{p,g,ca}$ and $C_{p,g,an}$ are the heat capacity of the gas at two electrodes. The atmospheric temperature T_0 is set as 303.15 K, and the lower heating value (LHV) is utilized to calculate these indicators [32].

The conversion ratio γ_{syn} represents the ratio of the electrolyzed steam to the input steam at the anode.

$$\gamma_{syn} = \frac{(X_{in,H_2O} - X_{out,H_2O})}{X_{i,H_2O}} \quad (16)$$

Here X_{in,H_2O} and X_{out,H_2O} represent the steam molar fractions of inlet and outlet.

3. Results and discussion

3.1 Effect of applied voltage

The current density distribution along the flow direction is shown in Fig.2a. As expected, the current density decreases along the flow channel, the higher the applied voltage, the more obvious the trend. Moreover, the electrochemical reaction rate is highly related to the anode gas composition, so the electrolysis reaction rate decreases with the decreasing anode water molar fraction. As shown in Fig.2b, the molar fraction of water decreases more significantly at a higher voltage (1.7V), leading to an obvious decrease of current density along the flow direction. Furthermore, the lowest reactant concentration at the anode outlet is prone to reactant starvation.

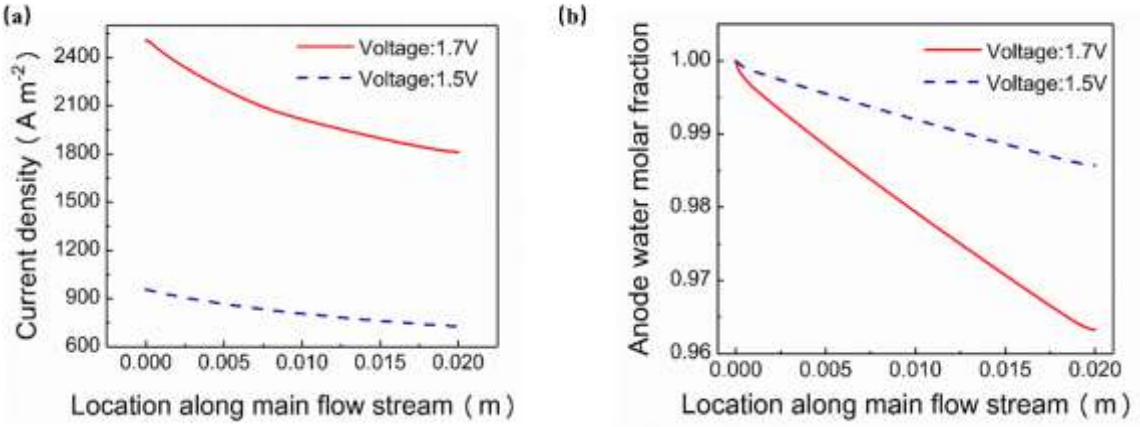

Fig.2 (a) Effect of applied voltage on current density along the flow direction; (b) Anode water molar fraction distribution at different voltages.

The heat generated by polarization losses and the heat consumption of electrochemical reaction affect temperature distribution of the HT-PEMEC and both heats increase with increasing voltage. As shown in Fig.3a, because the heat generation by irreversible processes is lower than the heat consumption for steam electrolysis reaction, the HT-PEMEC is under endothermic state, causing the temperature to decrease along the flow channel. As the applied voltage increase (to 1.47V and 1.48V), HT-PEMEC changes from an endothermic state to a thermally neutral state (Fig.3c), because electrochemical endothermic heat is equal to overpotential exothermic heat. The thermoneutral voltage (TNV) is critical for thermal management, meaning that the electrolyzer can maintain temperature without additional input and output heat. With the further increase of the applied voltage, the overpotential exothermic heat exceeds the electrochemical endothermic heat, resulting in an exothermic state of HT-PEMEC (Fig.3d and Fig.3e).

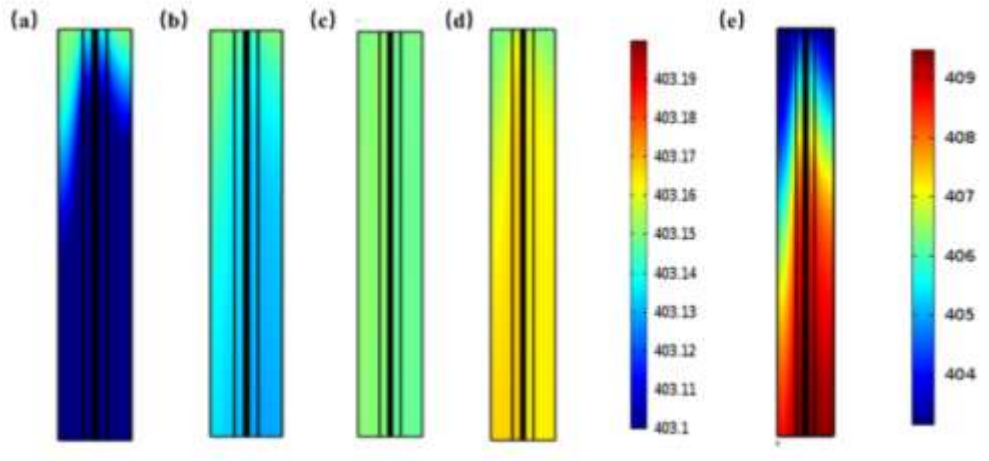

Fig.3 Distribution of temperature at 1.4V (a), 1.47V (b), 1.48V (c), 1.49V (d), and 1.7V(e).

To gain a fundamental understanding of the temperature distribution in the different components, the temperature distributions of the endothermic state and exothermic state are shown in Fig.4a and Fig.4b, respectively. The solid structure is composed of electrolyte, catalytic layers, and gas diffusion layers. It has high thermal conductivity, and the heat consumption and generation mainly occur in the solid structure, making the temperature change of the solid structure the most sensitive. On the other hand, the specific heat capacity of the cathodic gas is greater than that of anodic gas, so the temperature change of cathodic gas is more gently. Moreover, it is found that there is a maximum temperature difference at about a quarter of the channel length along the flow channel, which may cause thermal safety issues.

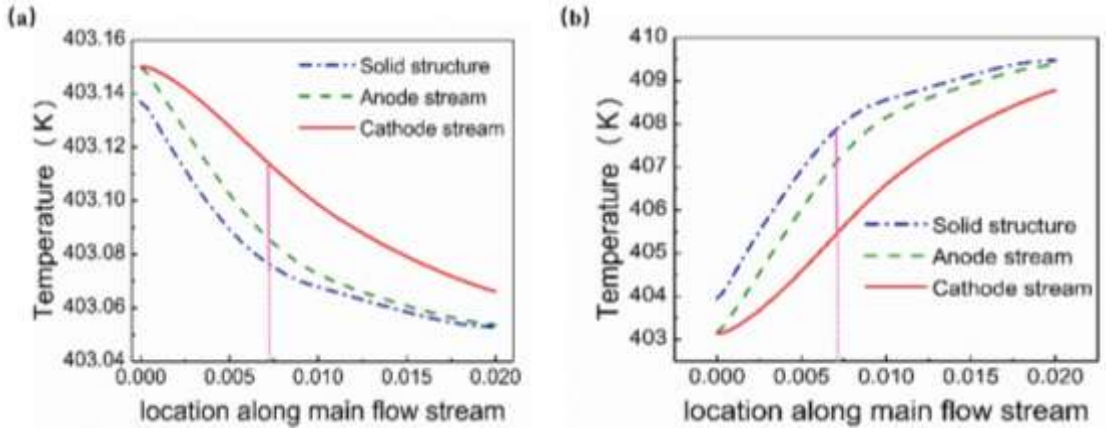

Fig.4 Effect of applied voltage on temperature distribution along the flow direction at

1.4V (a) and 1.7V (b).

As shown in Fig.5, the applied voltage affects the input electrical power and the chemical energy generated, while the energy required to preheat the gas remains unchanged. The electrical power is very small in comparison with the heat demand to heat the inlet gases of anode and cathode from ambient to the specified inlet temperature at a low voltage, and the generated hydrogen linearly varies with current density, leading to the increased energy efficiency with increasing voltage. However, the electrical power increases more significantly than the chemical energy of hydrogen at a high voltage, causing the overall efficiency to decrease with increasing voltage. Under the present simulation conditions, the optimal voltage to achieve peak energy efficiency is about 1.9V, and the detailed information on operating conditions is shown in Table 3. The increased current density allows more reactants to participate in the electrochemical reaction, resulting in an increased conversion rate.

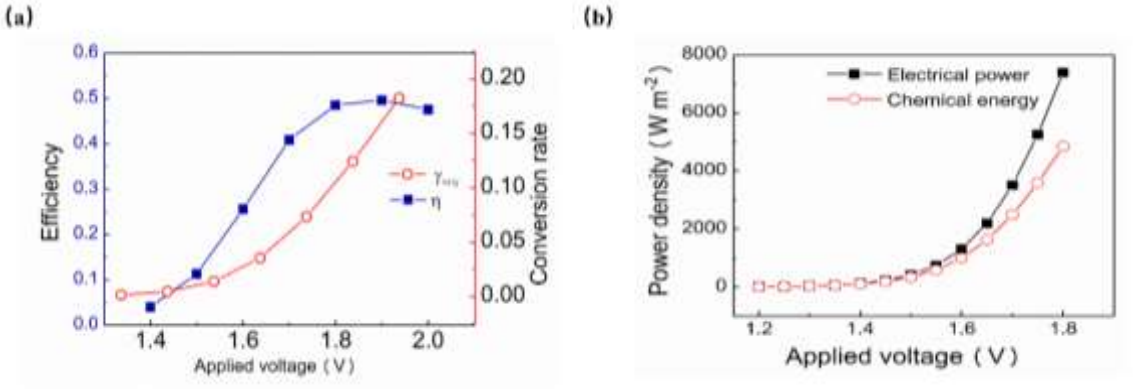

Fig.5 (a) Effect of applied voltage on efficiency and conversion ratio; (b) Effect of applied voltage on electrical power and chemical energy.

Table 3. Operation parameters for the study of applied voltage.

Parameters (unit)	Value
Applied voltage	1.4 -2 V
Anode water mass fraction	1
Cathode inlet gas velocity	0.4 m s^{-1}

Anode inlet gas velocity	0.1 m s^{-1}
Operating pressure	1 bar

3.2 Effect of anode gas composition

As shown in Fig.6, the effect of anode water mass fraction on the performance of the HT-PEMEC, then the detailed information of operating conditions are shown in Table 4. The input anode gas is composed of nitrogen and steam. As shown in Fig.6a, the increase in the mass fraction of anode water improves the concentration of reactants at the reaction interface, thereby increasing the current density. This behaviour indicates that a higher anode water mass fraction is desirable to produce more electrical energy. Fig.6b shows the effect of anode water mass fraction on the molar fraction of oxygen and hydrogen. It is found that the molar fractions of oxygen and hydrogen increase with increasing anode water mass fraction due to the enhanced electrochemical reaction.

Table 4. Operation parameters for the study of anode water mass fraction.

Parameters (Unit)	Value
Applied voltage	1.7 V
Anode water mass fraction	0.3-1
Cathode inlet gas velocity	0.4 m s^{-1}
Anode inlet gas velocity	0.1 m s^{-1}
Operating pressure	1 bar

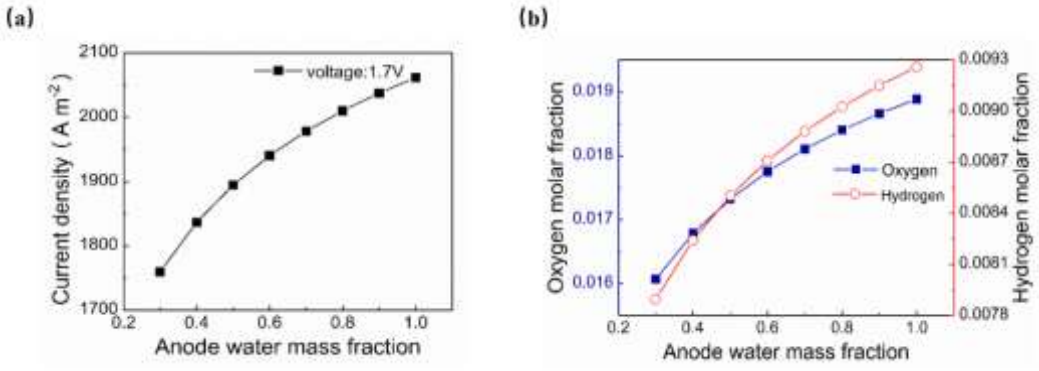

Fig.6 (a) Effect of inlet anode water mass fraction on performance of HT-PEMEC at 403K; (b) Effect of inlet anode water mass fraction on oxygen fraction and hydrogen molar fraction.

The anode water mass fraction directly affects the input electric energy, the chemical energy produced, and the heating gas energy. It can be found from Fig.7b that the specific heat capacity increases with the increasing mass fraction of anode water, which leads to the need for more energy to preheat the input gas. The effect of anode water mass fraction on the input electrical power and chemical energy generated (H_2 fuel) is shown in Fig.7c. It is worth noting that the increasing tendency of the generated chemical energy becomes smaller compared to the input electric power and the energy required to heat the gas when the steam mass fraction is greater than 0.6. Overall, the energy efficiency shows a trend of first reaches the peak value and then decreases. However, the conversion rate decreased due to excess steam.

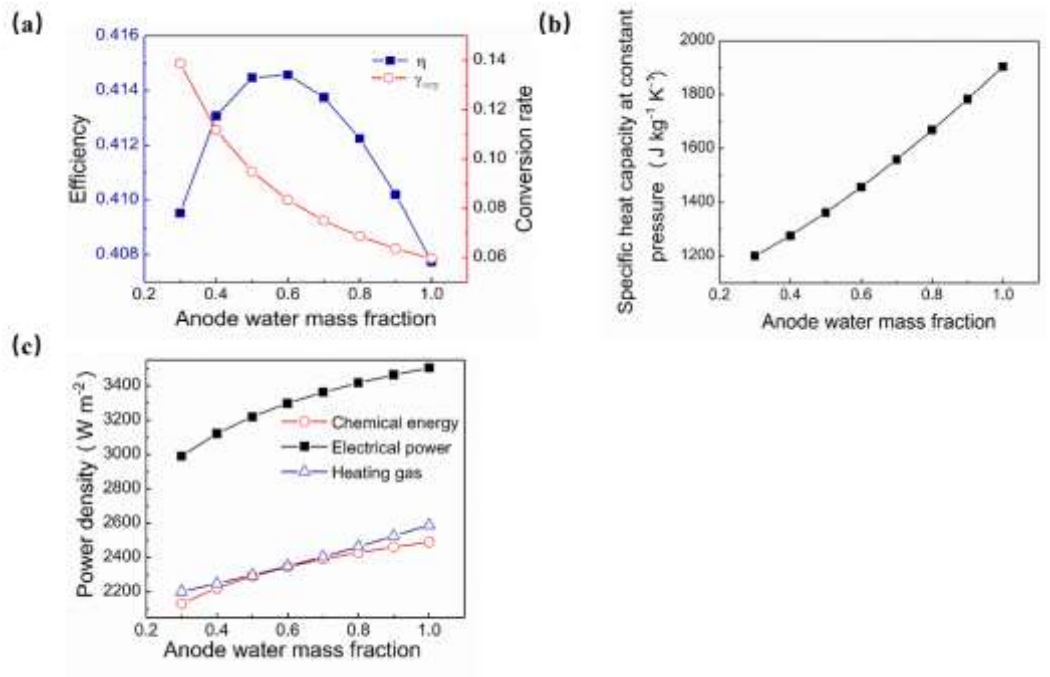

Fig.7 (a) Effect of inlet anode water mass fraction on efficiency and conversion ratio; (b) Effect of inlet anode water mass fraction on specific heat capacity at constant pressure; (c) Effect of inlet anode water mass fraction on output and input of power density.

3.3 Effect of cathode inlet gas velocity

The effect of the cathode inlet gas velocity on HT-PEMEC is shown in Fig.8a. As expected, the current density increases with increasing cathode inlet gas velocity, leading to a higher rate of electrolytic reaction. The detailed information on operating conditions is shown in Table 5. The average oxygen molar fraction and hydrogen molar fraction in steady states are presented in Fig.8b. it is found that the molar fraction of oxygen increases with increasing cathode inlet gas velocity due to the reinforced electrolytic reaction, but the hydrogen is diluted by supplied steam resulting in a downward trend in hydrogen molar fraction.

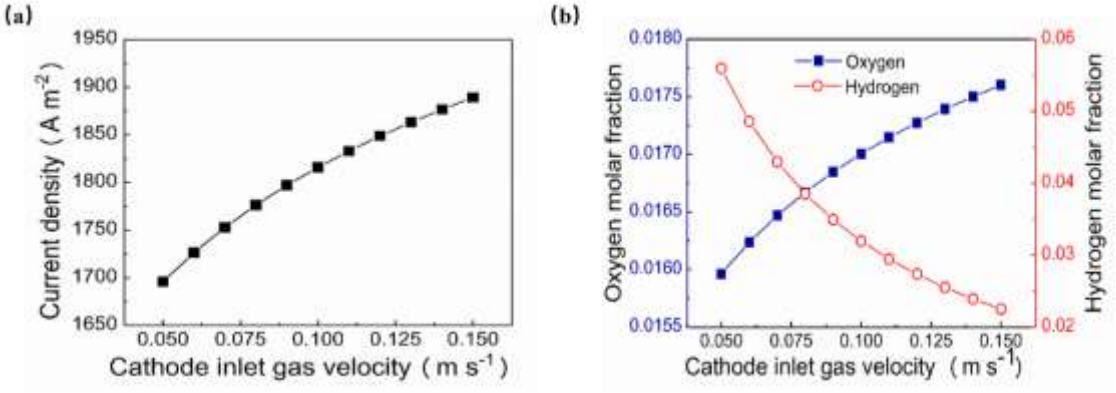

Fig.8 (a) Effect of cathode inlet gas flow rate on current density; (b) Effect of cathode inlet gas flow rate on the fraction of oxygen and hydrogen.

Table 5. Operating parameters for the study of cathode inlet gas velocity.

Parameters (Unit)	Value
Applied voltage	1.7 V
Anode water mass fraction	1
Cathode inlet gas velocity	0.05-0.15 m s^{-1}
Anode inlet gas velocity	0.1 m s^{-1}
Operating pressure	1 bar

The electrochemical reaction and heat exchange is affected by the cathode gas velocity to

change the operating temperature. Fig.9b and Fig.9c show the effect of cathode inlet gas velocity on heat generation and net heat. The heat generated by the irreversible loss and the heat consumed by the electrochemical reaction rise with increasing cathode gas velocity, but overall it manifests an increase in net heat release. However, the increase in cathode gas velocity takes away more heat inside the electrolyzer. Therefore, the average temperature of the HT-PEMEC rises first and then decreases as the cathode gas velocity increases, as shown in Fig.9a.

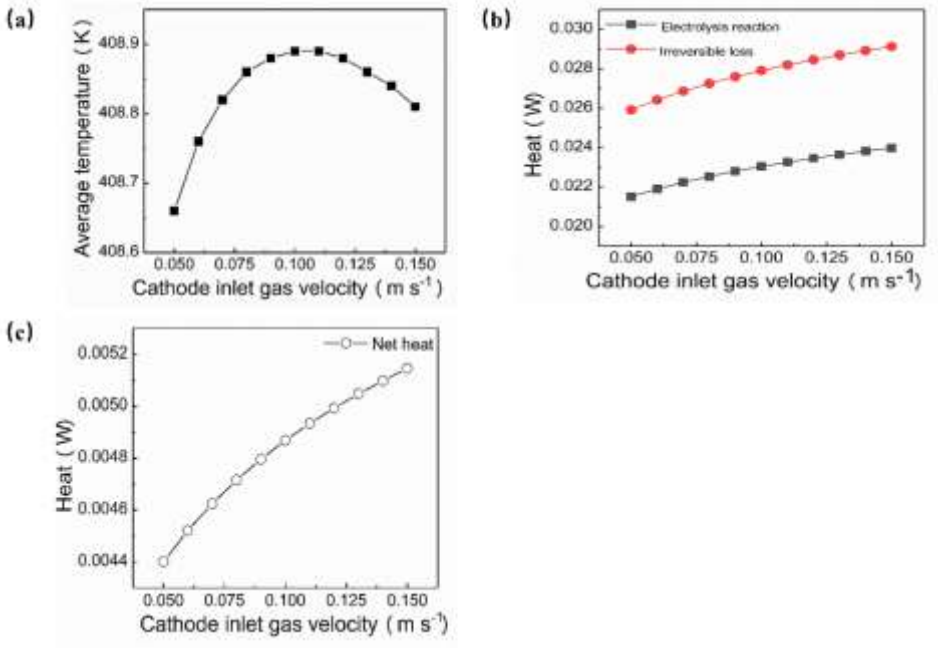

Fig.9 (a) Effect of cathode inlet gas velocity on average temperature; (b) Effect of cathode inlet gas velocity on heat; (c) Effect of cathode inlet gas velocity on net heat.

As shown in Fig.10b, the cathode inlet gas velocity affects the input electrical power, chemical energy generated, and heating gas energy. The increase in cathode inlet gas velocity not only promotes the electrochemical reaction but also requires more energy to preheat the gas. The overall efficiency is shown in Fig.10a, showing a trend of first rising and then falling. Moreover, the conversion rate is increased due to the reinforced electrochemical reaction consumes more steam.

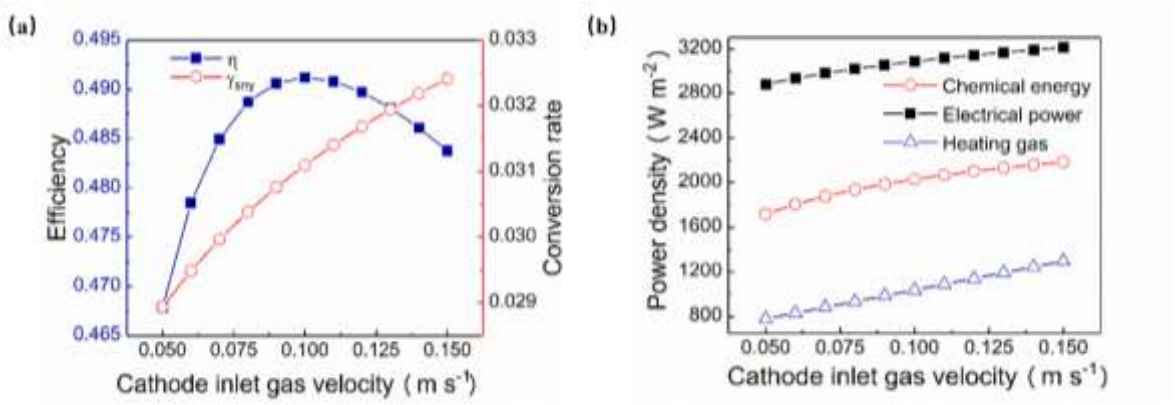

Fig.10 (a) Effect of cathode inlet gas velocity on efficiency and conversion ratio; (b) Effect of cathode inlet gas velocity on output and input of power density.

3.4 Effect of anode inlet gas velocity

The inlet gas velocity of the anode is varied from 0.05m/s to 1.5m/s to examine its effect on the HT-PEMEC performance. More detailed information about operating conditions is shown in Table 6. It can be observed from Fig.11a that the current density of the HT-PEMEC increases with increasing anode inlet gas velocity because it not only reduces the concentration of oxygen generated but also alleviates the drop in steam concentration. The impact of anode inlet gas velocity on the concentration of hydrogen and oxygen in the electrolyzer is shown in Fig.11b. The hydrogen molar fraction increases due to the reinforced electrochemical reaction, while the oxygen is diluted by the supplied steam.

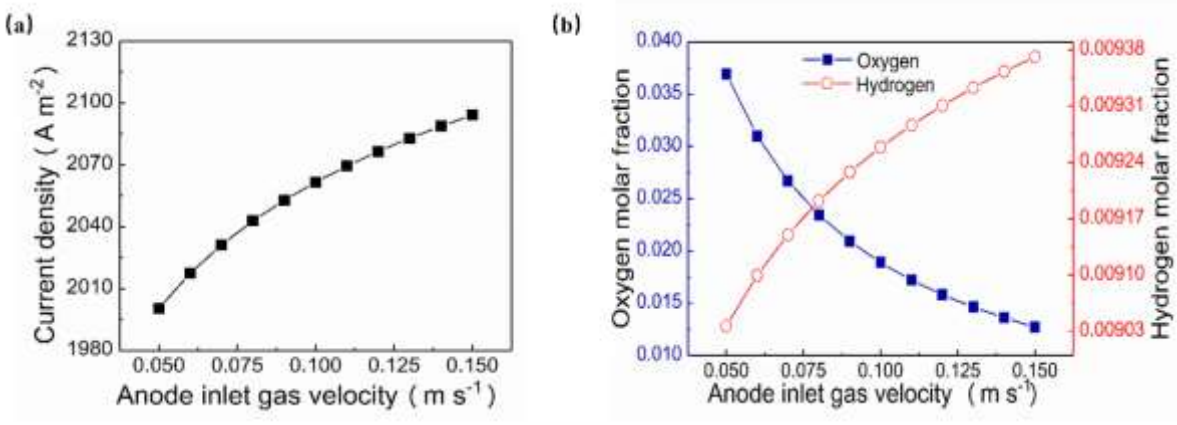

Fig.11 (a) Effect of anode inlet gas velocity on current density; (b) Effect of anode inlet

gas velocity on the molar fraction of oxygen and hydrogen.

Table 6. Operating parameters for the study of anode inlet gas velocity.

Parameters (Unit)	Value
Applied voltage	1.7 V
Anode water mass fraction	1
Cathode inlet gas velocity	0.4 m s^{-1}
Anode inlet gas velocity	0.05-0.15 m s^{-1}
Operating pressure	1 bar

The impact of the anode inlet gas velocity on the operating temperature is similar to that of the cathode inlet gas velocity. The increase in anode inlet gas velocity increases the heat generation by irreversible loss and heat consumption by the electrochemical reaction, but overall it shows an increase in net heat release (Fig.12b). However, the increase in anode inlet gas velocity takes away more heat inside the electrolyzer. Therefore, the average temperature of the HT-PEMEC rises first and then decreases as the anode gas velocity increases, as shown in Fig.12a.

The anode inlet gas velocity affects the input electrical power, and the chemical energy generated and heating gas energy by changing the electrochemical reaction and anode input gas flux. As shown in Fig.12c and Fig.12d, the output chemical energy, input electrical power, and input heating energy increase with increasing anode gas velocity, but the overall efficiency decreases. Moreover, the conversion rate is reduced due to the excess steam supply.

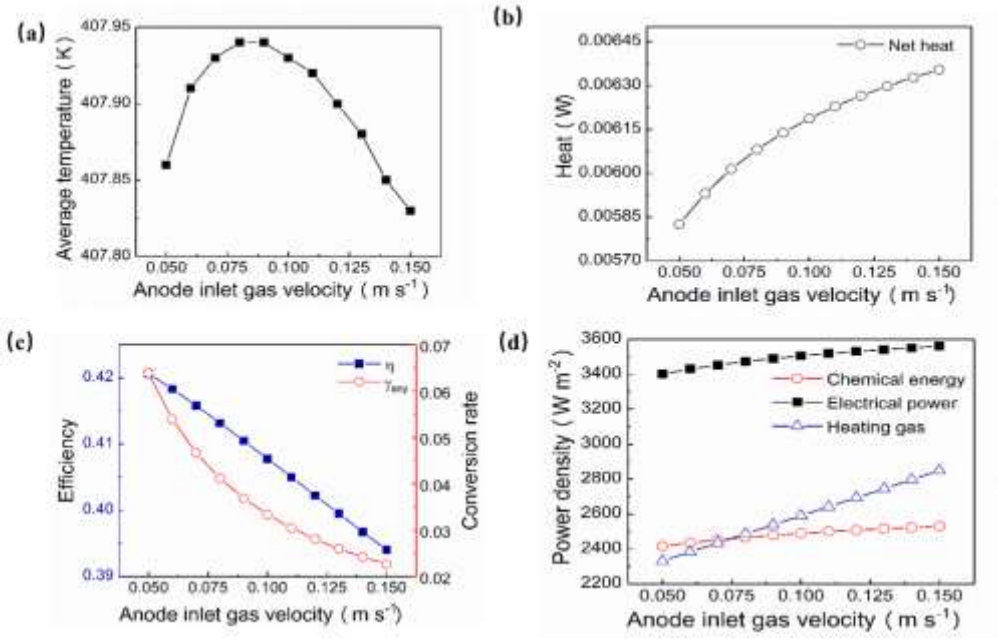

Fig.12 (a) Effect of anode inlet velocity on average temperature; (b)Effect of anode inlet gas velocity on net heat; (c) Effect of anode inlet gas velocity on efficiency and conversion ratio; (d) Effect of anode inlet gas velocity on output and input of power density.

3.5 Steady-state optimal operating point

The HT-PEMEC performance depends on multiple operating variables (applied voltage, anode water mass fraction, cathode inlet gas velocity and anode inlet gas velocity) and the corresponding overall performance of HT-PEMEC can be obtained by simulating each operation point. Moreover, the optimal operating point can be found by solving the optimization problem by the Nelder-Mead method.

$$\max(\eta) \tag{18}$$

Table 7. Operating parameter range and constraints.

Parameters (Unit)	Parameter	Precision
Applied voltage	V (1.4-2 V)	0.01

Anode water mass fraction	0.3-1	0.01
Anode gas velocity	0.03-0.15 m s^{-1}	0.01
Cathode gas velocity	0.03-0.15 m s^{-1}	0.01
Local steam mole fraction	$X_{local,H_2O} > 0$	
Constraint resolution	Augmented lagrangian	
Constraint tolerance	0.01	

Based on Eq.18, the optimal operating point can be found as the following processes:

(1) Initializing the boundaries of parameters as shown in Table 7. Because there are enormous different combinations in the operation range, each variable parameter is discretized with a certain precision according to the range of operating conditions and the required calculation amount.

(2) Nelder-Mead optimization method is used. The Nelder-Mead method depends on a simplex of M+1 points, where M is the number of control variables. Through the Nelder-Mead method iteration, the solver uses reflection, expansion and contraction to improve the worst point in the simplex, and the radius of the simplex is reduced. The optimal point is found when the radius approaches zero. The advantage of the Nelder-Mead method is that the derivative of the objective function is not used, thereby simplifying the calculation process.

(3) Obtaining the operating point with maximum efficiency. This process can be formulated to solve the objective function, and the constraint is that the local water molar fraction should be greater than zero, otherwise it will cause the reactants starvation problem.

Through the above solving process, the optimal operating point can be obtained in table 8. The maximum efficiency of the HT-PEMEC is 54.5% and the steam conversion ratio is 35.4%.

Table 8. Optimal operating conditions.

Objective	Applied voltage	Anode water mass fraction	Anode gas velocity	Cathode gas velocity	value
Max(η)	1.76 V	0.44	0.03 m s^{-1}	0.11 m s^{-1}	54.5 %

4. Conclusions

In the paper, a 2D multiphysics model is developed to investigate the electrolysis reaction, protonic and electronic charge transport process, mass transport process and momentum transport process. Furthermore, the steady-state model is used to predict the performance and optimal operating point of the HT-PEMEC.

The influence of applied voltage, anode water mass fraction, cathode inlet gas velocity and anode inlet gas velocity on the multiphysics field of the electrolyzer was studied. It is found that the electrolyzer transfers from endothermic state to exothermic state with increasing applied voltage, and the TNV is observed to be 1.48V. Furthermore, It is found that applied voltage, cathode inlet gas velocity, and anode inlet gas velocity affect the overall efficiency more significantly while the anode water mass fraction has less effect on energy efficiency. As the applied voltage increases, the overall efficiency rises first and then falls while the conversion ratio increases. The effect of anode water mass fraction on overall efficiency is the same as the applied voltage while the conversion ratio decreases with increasing anode mass fraction. anode and cathode inlet gas velocities have the same trend on average temperature, which rises first and then falls with increasing gas velocity, while the effect on overall efficiency and conversion ratio is different. As cathode inlet gas velocity increases, the overall efficiency rises first and then falls while the conversion ratio increases. However, the overall efficiency and conversion

ratio decreases with increasing anode inlet gas velocity. Current research work also predicts the performance of different operating conditions and the optimal operating point of the HT-PEMEC is evaluated.

Declaration of competing interest

The authors declare that they have no known competing financial interests or personal relationships that could have appeared to influence the work reported in this paper.

Acknowledgements

The authors would like to thank the support from National Natural Science Foundation of China (61873323, 61773174, 61573162), the Wuhan science and technology plan project (2018010401011292). M. Ni thanks the funding support from Research Grant Council (Project Number: PolyU 152214/17E), University Grants Committee, Hong Kong SAR.

References

[1] A roadmap for moving to a competitive low carbon economy in 2050. European Commission; 2011 [COM(2011) 112/F].

[2] Yu J, Ran R, Zhong Y, et al. Advances in Porous Perovskites: Synthesis and Electrocatalytic Performance in Fuel Cells and Metal–Air Batteries[J]. Energy & Environmental Materials.2020. 3(2), 121-145.

[3] Bensmann B, Hanke-Rauschenbach R, Arias I K P, et al. Energetic evaluation of high pressure PEM electrolyzer systems for intermediate storage of renewable energies. Electrochimica Acta, 2013, 110: 570-580.

[4] Yu J, Zhong Y, Wu X, et al. Bifunctionality from synergy: CoP nanoparticles embedded in amorphous CoOx nanoplates with heterostructures for highly efficient water electrolysis. Advanced Science, 2018, 5(9): 1800514.

[5] Yu J, He Q, Yang G, et al. Recent advances and prospective in ruthenium-based materials for electrochemical water splitting[J]. Acs Catalysis, 2019, 9(11): 9973-10011.

[6] Ahmadi N, Rezazadeh S, Dadvand A, et al. Numerical investigation of the effect of gas diffusion layer with semicircular prominences on polymer exchange membrane fuel cell performance and species distribution[J]. Journal of Renewable Energy and Environment, 2015, 2(2): 36-46.

[7] Ahmadi N, Rostami S. Enhancing the performance of polymer electrolyte membrane fuel cell by optimizing the operating parameter[J]. Journal of the Brazilian Society of Mechanical Sciences and

Engineering, 2019, 41(5): 1-19.
[8] Jabbary A, Rostami Arnesa S, Samanipour H, et al. Numerical investigation of 3D rhombus designed PEMFC on the cell performance[J]. International Journal of Green Energy, 2021, 18(5): 425-442.
[9] Ahmadi N, Kõrgesaar M. Analytical approach to investigate the effect of gas channel draft angle on the performance of PEMFC and species distribution[J]. International Journal of Heat and Mass Transfer, 2020, 152: 119529.
[10] Tijani AS, Rahim AHA. Numerical modeling the effect of operating variables on Faraday efficiency in PEM electrolyzer. Procedia Technol 2016;26:419-27.
[11] Bessarabov D, Wang H, Li H, Zhao N. PEM electrolysis for hydrogen production: principles and applications. CRC Press; 2016.
[12] Carmo M, Fritz D L, Mergel J, et al. A comprehensive review on PEM water electrolysis[J]. International journal of hydrogen energy, 2013, 38(12): 4901-4934.
[13] Grigoriev S A, Porembsky V I, Fateev V N. Pure hydrogen production by PEM electrolysis for hydrogen energy[J]. International Journal of Hydrogen Energy, 2006, 31(2): 171-175.
[14] Linkous CA, Anderson HR, Kopitzke RW, Nelson GL. Development of new proton exchange membrane electrolytes for water electrolysis at higher temperatures. Int J Hydrogen Energy 1998;23:525-9.
[15] Nikiforov A, Christensen E, Petrushina I, Jensen JO, Bjerrum NJ. Advanced construction materials for high temperature steam PEM electrolysers. INTECH Open Access Publisher; 2012.
[16] Hansen MK, Bjerrum N, Christensen E, Jensen JO. PEM water electrolysis at elevated temperatures. Ph.D. thesis. Technical University of Denmark, Department of Chemistry Institut; 2012.
[17] Ruiz D D H, Sasmito A P, Shamim T. Numerical investigation of the high temperature PEM electrolyzer: effect of flow channel configurations. ECS Transactions, 2013, 58(2): 99-112.
[18] Toghyani S, Afshari E, Baniasadi E, et al. Thermal and electrochemical performance assessment of a high temperature PEM electrolyzer. Energy, 2018, 152: 237-246.
[19] Santarelli M, Medina P, Calì M. Fitting regression model and experimental validation for a high-pressure PEM electrolyzer. International Journal of Hydrogen Energy, 2009, 34(6): 2519-2530.
[20] Nafchi F M, Baniasadi E, Afshari E, et al. Performance assessment of a solar hydrogen and electricity production plant using high temperature PEM electrolyzer and energy storage[J]. International Journal of Hydrogen Energy, 2018, 43(11): 5820-5831.
[21] Tijani AS, Barr D, Rahim AHA. Computational modelling of the flow field of an electrolyzer system using CFD. Energy Procedia 2015;79:195-203.
[22] Ni M. 2D thermal modeling of a solid oxide electrolyzer cell (SOEC) for syngas production by H2O/CO2 co-electrolysis. International Journal of Hydrogen Energy, 2012, 37(8): 6389-6399.
[23] Xu H, Chen B, Irvine J, et al. Modeling of CH4-assisted SOEC for H2O/CO2 co-electrolysis. International Journal of Hydrogen Energy, 2016, 41(47): 21839-21849.
[24] Costamagna P, Honegger K. Modeling of solid oxide heat exchanger integrated stacks and simulation at high fuel utilization. J Electrochem Soc 1998;145:3995-4007.
[25] Ni M. An electrochemical model for syngas production by co- electrolysis of H2O and CO2. J Power

Sources 2012;202:209-16.
[26] Suwanwarangkul R, Croiset E, Fowler MW, Douglas PL, Entchev E, Douglas MA. Performance comparison of Fick's, dusty-gas and StefaneMaxwell models to predict the concentration overpotential of a SOFC anode. J Power Sources 2003;122:9-18.
[27] Chan SH, Khor KA, Xia ZT. A complete polarization model of a solid oxide fuel cell and its sensitivity to the change of cell component thickness. J Power Sources 2001;93:130-40.
[28] Todd B, Young JB. Thermodynamic and transport properties of gases for use in solid oxide fuel cell modelling. J Power Sources 2002;110:186-200.
[29] Kakaç S, Pramuanjaroenkij A, Zhou XY. A review of numerical modeling of solid oxide fuel cells. Int J Hydrogen Energy 2007;32:761-86.
[30] Xu H, Chen B, Zhang H, et al. The thermal effect in direct carbon solid oxide fuel cells. Applied Thermal Engineering, 2017, 118: 652-662.
[31] He Q, Yu J, Xu H, et al. Thermal effects in H2O and CO2 assisted direct carbon solid oxide fuel cells[J]. International Journal of Hydrogen Energy, 2020;45(22):12459-75.
[32] Luo Y, Shi Y, Li W, et al. Comprehensive modeling of tubular solid oxide electrolysis cell for co-electrolysis of steam and carbon dioxide. Energy, 2014, 70: 420-434.
[33] Hansen M K, Aili D, Christensen E, et al. PEM steam electrolysis at 130° C using a phosphoric acid doped short side chain PFSA membrane. International Journal of Hydrogen Energy, 2012, 37(15): 10992-11000.
[34] Zhao D, He Q, Yu J, et al. Dynamic behaviour and control strategy of high temperature proton exchange membrane electrolyzer cells (HT-PEMECs) for hydrogen production[J]. International Journal of Hydrogen Energy, 2020, 45(51): 26613-26622.
[35] Li H, Nakajima H, Inada A, et al. Effect of flow-field pattern and flow configuration on the performance of a polymer-electrolyte-membrane water electrolyzer at high temperature[J]. International Journal of Hydrogen Energy, 2018, 43(18): 8600-8610.
[36] Li H, Inada A, Fujigaya T, et al. Effects of operating conditions on performance of high-temperature polymer electrolyte water electrolyzer[J]. Journal of Power Sources, 2016, 318: 192-199.
[37] Toghyani S, Baniasadi E, Afshari E. Numerical simulation and exergoeconomic analysis of a high temperature polymer exchange membrane electrolyzer[J]. International Journal of Hydrogen Energy, 2019, 44(60): 31731-31744.
[38] Xu W, Scott K, Basu S. Performance of a high temperature polymer electrolyte membrane water electrolyser [J]. Journal of Power Sources, 2011, 196(21): 8918-8924.